MATISSE Consortium

OCA-UNS-CNRS, Nice, France
MPIA, Heidelberg, Germany
MPIfR, Bonn, Germany
NOVA, The Netherlands
ITAP, Kiel University, Germany
Vienna University, Vienna, Austria

Very Large Telescope

MATISSE

Inspection and Test Report Detector

Doc. No.: VLT-TRE-MAT-15860-9133

Issue: 2.1

Date: 18.07.2017

Author(s):	U. Beckmann	18.07.2017	
	Name	Date	
Project Manager:	P. Antonelli	18.07.2017	
	Name	Date	Signature
Principal Investigator:	B. Lopez	18.07.2017	
	Name	Date	Signature

* Co-authors: Matthias Heininger

CHANGE RECORD

ISSUE	DATE	SECTION/PAGE AFFECTED	REASON/INITIATION/DOCUMENT/REMARKS
1	10.11.2016	All	First issue
2	24.05.2017	3, 4	Extended and updated
2.1	18.07.2017	3.2 .. 3.5, 3.11	Images of all four bad pixel maps included, plot of HAWAII-2RG non-linearity added

TABLE OF CONTENTS

List of Figures

List of Tables

1 SCOPE, APPLICABLE AND REFERENCE DOCUMENTS

1.1 Scope

As described in the MAIT plan [AD3], the test and verification program of MATISSE results in the PAE of MATISSE. However, sub-system verifications reduce risk and improve knowledge of the system prior to the full systems verification.
This document describes the tests and verification of the detector (DET) sub-systems. It first gives the test results on the global sub-systems, then of the modules, and finally checks the component compliance.
The test results show that the DET complies with the low level specifications and conduct to its acceptance.
The end of the test and verification program of the WOP is marked by the MATISSE Readiness Review MRR9.

1.2 Applicable Documents

The following Applicable Documents (AD) of the exact issue form part of the present document.

AD Nr	Doc Nr	Doc Title	Issue	Date
AD1	VLT-SPE-MAT-15860-9004	MATISSE Instrument specifications	3	19/10/2011
AD2	VLT-TRE-MAT-15860-9101	MATISSE Design and Performance Report: Optics (Warm Optics)	5	10/11/2016
AD3	VLT-PLA-MAT-15860-9050	MATISSE MAIT	6	31/07/2012
AD4	VLT-MAN-MAT-15860-9xxx	MATISSE Optical Alignment Manual		10/11/2016
AD5	VLT-ICD-MAT-15860-9005	MATISSE Internal Interface Document	5	31/07/2012
AD 6	MAT-SYS-VRM001	Verification matrix		
AD 7	MATISSE-MPIA-TN-023	Cryostat temperature characteristics	1.1	17/05/2017

1.3 Reference Documents

The following Reference Documents (RD) contains information relevant to the present document.

RD Nr	Doc Nr	Doc Title	Issue	Date
RD1	MATISSE-OCA-TN-007	Manufacturing report of the optical components of the Warm Optics	1	10/11/2016
RD2	MATISSE-OCA-TN-005	CMO: Angular stability	1	12/06/2013
RD3	MATISSE-OCA-TN-006	Targets: positioning measurements	1	29/08/2013
RD4	MATISSE-OCA-TN-008	WOP modules integration	1	10/11/2016
RD5	VLT-TRE-MAT-15860-9xxx	MATISSE Instrument and Performance Report	1	10/11/2016

2 Test results of the L/M-Band and N-Band Detectors

The following table lists all detector related requirements from the verification matrix. Some requirements are fulfilled by the detector itself or by the MATISSE hardware and software (design). Most of the requirements were tested using data taken with the MATISSE instrument.

Name	ID	Verification /Method	Detector, Configuration	Desired value	Actual value
Crosstalk between pixels	6.08	T/T	L-Band, spatial	< 2.5 %	1.3 % (100 kHz), 3.4 % (2 MHz)
			L-Band, spectral	< 5 %	2.8 % (100 kHz), 1.8 % (2 MHz)
			N-Band, spatial	< 2.5 %	8.1 % (high gain, 2.4 MHz), 3 % (high gain, 1.7 MHz), 9.8 % (low gain, 2.4 MHz)
			N-Band, spectral	< 5 %	4.8 % (high gain, 2.4 MHz), 6.2 % (low gain, 2.4 MHz)
Detector vibration, spatial direction	6.09	T/A	L-Band	< 1.8 µm PTV	
			N-Band	< 3.5 µm PTV	< 1.7 µm @ 1 - 100 Hz
Detector window	8.01	T/D	L-Band	P ≥ 75 px, I ≥ 450 px, @ 5 µm	Yes (***)
			N-Band	P ≥ 78 px, I ≥ 468 px, @ 13 µm	Yes (***)
OPD Modulation	9.02	T/D		sync accuracy < 1 ms	Yes (***)
Detector temperature	10.27	T/T	L-Band	40 K, stability < 0.1 K	40 K, < 0.05 K
	10.28		N-Band	6..10 K, stability < 0.1 K	9 K, < 0.001 K
Preamp temperature	10.29	T/T	L-Band	40 - 120 K	60 - 80 K
Dark current (stray light)	11.07	T/T	L-Band, 100 kHz	< RON^2 (10^2)	1 e-/s → 100 s
			L-Band, 2 MHz	< RON^2 (63^2)	1 e-/s → 3200 s
			N-Band, low gain	< RON^2 (1800^2)	13000 e-/s → 250 s
			N-Band, high gain	< RON^2 (210^2)	13000 e-/s → 3 s
Detector QE	12.01	T/D	L-Band	> 50 %	> 70 % (*)
	12.02		N-Band	> 50 %	> 50 % (*)
Readout noise	12.03	T/T	L-Band, 100 kHz	< 15 e-	10.1 e-
			L-Band, 2 MHz		53.5 e-
	12.04		N-Band, low gain		1800 e-
			N-Band, high gain	< 300 e-	210 e-
Spectral Range	12.05	T/D	L-Band	2.8 – 5 µm	2.8 - 5 µm (*)
	12.06		N-Band	8 - 13 µm	5 – 25 µm (*)
Detector integration time	12.07	T/D	L-Band, without FT	30 – 75 ms	Yes (***)
			L-Band, with FT	Up to 2 min	Yes (***)
	12.08	T/D	N-Band, low gain	20 – 30 ms	> 50 µs, Yes (***)
			N-Band, high gain		> 50 µs, Yes (***)

Name	ID	Verification /Method	Detector, Configuration	Desired value	Actual value
Image configuration	12.09	T/D		1 – 5 images	Yes (***)
Readout direction	12.10	D/D		fast = spatial	Yes (***)
Image size	12.11	T/D		different sizes depending on the spectral resolution	Yes (***)
Array size	12.12	D/D	L-Band	2048x2048	2048x2048 (*)
			N-Band	1024x1024	1024x1024 (*)
Pixel size	12.13	D/D	L-Band	18 µm square	18 µm square (*)
			N-Band	30 µm square	30 µm square (*)
Full well capacity	12.14	T/A	L-band, 100 kHz	≥ 100000 e-	120000 e-
			L-Band, 2 MHz		130000 e-
	12.15		N-band, low gain	≥ 6000000 e-	9000000 e-
			N-band, high gain	≥ 600000 e-	> 960000 e-
Linearity, compensated	12.16	T/T	L-Band, 100 kHz	> 99 %	96000 e-
			L-Band, 2 MHz		100000 e-
	12.17		N-Band, low gain		6000000 e-
			N-Band, high gain		960000 e-
Dark current	12.18	T/T	L-Band, 100 kHz	< 5 e-/s	< 1 e- @ 40 K (measured)
			L-Band, 2 MHz		< 1 e- @ 40 K (measured)
	12.19		N-Band	< 1000 e-/s	3600 e- (measured) 200 e- @ 8.5 K (datasheet)
Remanence	12.24	T/T	L-Band	< 2 % (4τ)	τ = 2 ms, a 8 ms delay needed to reach the specification
	12.25		N-Band		τ = 5 ms, a 20 ms delay needed to reach the specification
Conversion Gain	12.26	T/T+A	L-Band, 100 kHz		2.73 e-/DU
			L-Band, 2 MHz		2.60 e-/DU
	12.27		N-Band, low gain		20 e-/DU (**)
			N-Band, high gain		190 e-/DU (**)
Electronic Gain	12.28	T/D	L-Band	Amplifier gain from detector output to input ADC	8
	12.29		N-Band		3
Correlated Noise	12.30	T/T	L-Band	Below RON	no correlated noise detected in power spectra
	12.31		N-Band		no correlated noise detected in power spectra
ELFN	12.32	T/-	L-Band	Below photon noise when averaged over 1 s	measurements suffered from detector non linearity
	12.33		N-Band		
Preamplifier	12.34	T/T+A	L-Band	Below RON	< 7 e- (1/2 of the total RON)

Name	ID	Verification /Method	Detector, Configuration	Desired value	Actual value
Noise	12.35		N-Band		100 e- (measurements without photon sensitivity)
Fixed pattern noise temporal stability	12.36	T/T	L-Band		75 s (Allan variance)
	12.37		N-Band		50 s (Allan variance)
Bad pixel map	12.38	T/T	L-Band, 100 kHz	No clusters of more than 2 pixel in spatial direction	3 large loose clusters, 67 compact clusters (3 or more bad pixels), 253 doublets
			L-Band, 2 MHz		3 large loose clusters, 275 compact clusters (3 or more bad pixels), 3449 doublets
	12.39		N-Band, low gain		29 compact clusters (3 or more bad pixels), 19 doublets
			N-Band, high gain		67 compact clusters (3 or more bad pixels), 38 doublets
Masked area	12.40	T/T	L-Band	32x128 pixels	left=80, right=80, bottom=30, top=40
			N-Band	32x32 pixels	left=32, right=32, bottom=32, top=31

Table 1: Detector Requirements, (*) values taken from data sheets, (**) calculated, (***) by design

3 Tests

3.1 Data sheet and design decisions

Some values of both detectors are given in the data sheets from Teledyne/Raytheon:

- Detector QE:
  - L-Band (12.01): > 70 % between 0.8 and 4.4 µm
  - N-Band (12.02): > 50 % between 8.9 and 25 µm
- Spectral Range:
  - L-Band (12.05): 2.8 - 5 µm
  - N-Band (12.06): 3 – 25 µm
- Readout direction (12.10): fast = spatial (horizontal)
- Array size (12.12):
  - L-Band: 248x2048 pixels
  - N-Band: 1024x1024 pixels
- Pixel size (12.13):
  - L-Band: 18 µm square
  - N-Band: 30 µm square

Some requirements were fulfilled by design decisions (hardware and software):

- Detector window (8.01): The DCS supports the required sub-window setup
- OPD-Modulation (9.02): The OPD modulator and detectors are triggered via TIM boards
- Image configuration (12.09): The DCS supports the required sub-window setup
- Image size (12.11): The DCS supports the required sub-window setup

3.2 HAWAII-2RG Detector characterization using the slow pixel clock

A set of cold dark and flat field exposures was taken with the *MATISSE_gen_cal_det_L_SLOW* OB. The associated MATISSE DRS plug-in *mat_cal_det* was used to calculate the bad pixel map, flat field map and nonlinearity map for the HAWAII-2RG detector at slow speed (100 kHz pixel clock). In addition some characteristic properties were calculated from the plug-in:

- Conversion factor (12.26): 2.73 e-/DU
- Readout noise (12.03): 10.1 e-
- Bad pixels: 8696 bad pixels of 2048x2048 pixels
- MINDIT: 1.382 s for the whole detector
- Full well capacity (12.14): > 120000 e-
- Nonlinearity compensation (12.16): up to 96000 e- possible, max residual 1 %
- Dark current (12.18): 0.022 e-/s (data sheet), < 1 e-/s (estimated, include stray light)
- Masked area (12.40): left=80, right=80, bottom=30, top=40

The HAWAII-2RG detector shows 67 compact clusters of at least 3 bad pixels and three loose clusters of bad pixels:

- a large loose cluster at (294,1907), 32 pixel diameter, 167 bad pixels
- a large loose cluster at (327,1092), 26 pixel diameter, 123 bad pixels
- a large loose cluster at (1634,1224), 50 pixels diameter, 127 bad pixels
- 253 clusters of 2 bad pixels
- 25 clusters of 3 bad pixels
- 12 cluster of 4 bad pixels
- 7 clusters of 5 bad pixels
- 4 clusters of 6 bad pixels
- 4 clusters of 7 bad pixels
- 3 clusters of 8 bad pixels
- 2 clusters of 9 bad pixels
- 2 clusters of 11 bad pixels
- 2 clusters of 12 bad pixels
- single cluster with 15, 20, 24, 30, 34 and 51 bad pixels

The following image shows the bad pixel map estimated from data taken in Nice, 15. July, 2016.

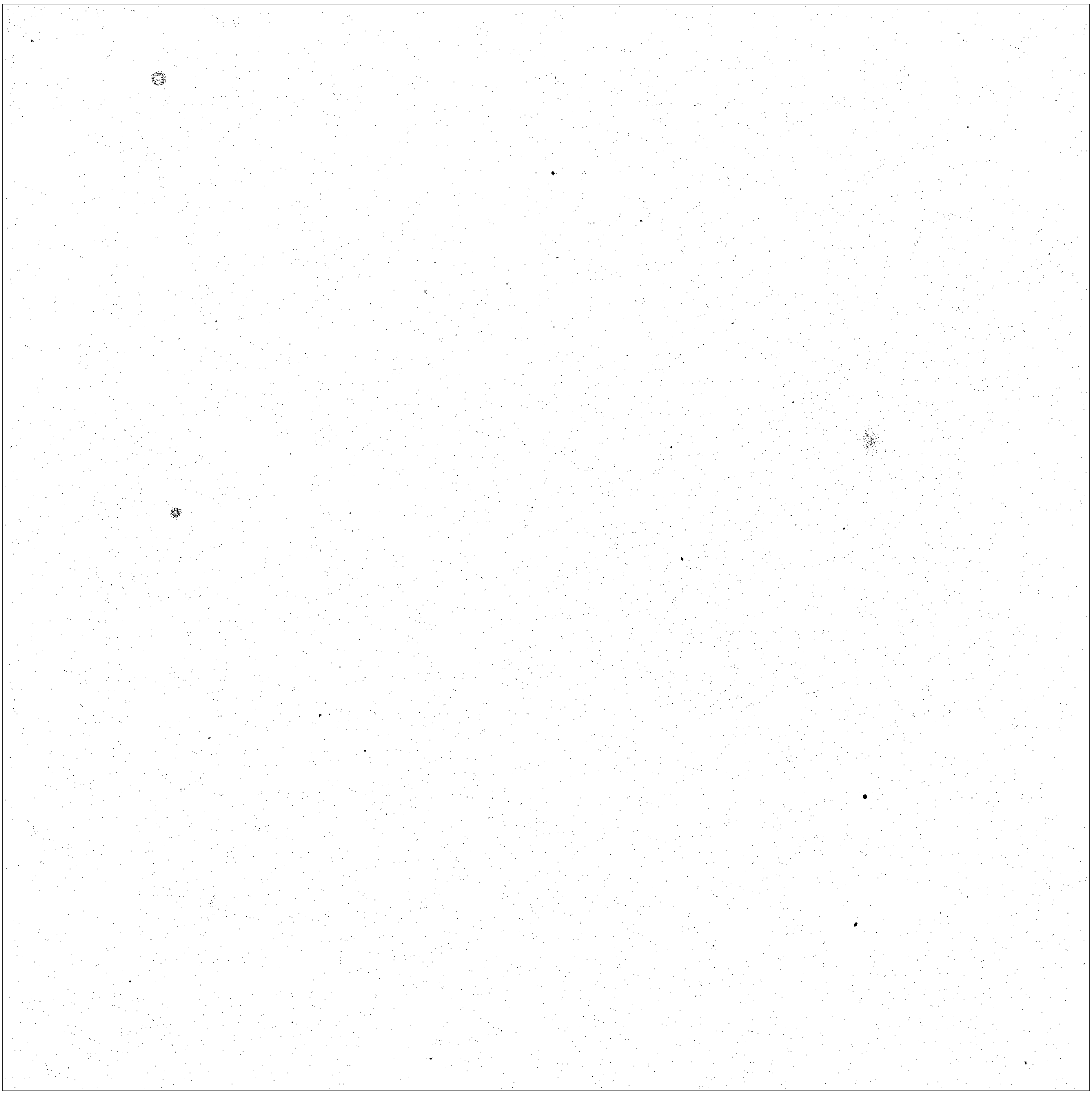

Illustration 1: HAWAII-2RG bad pixel map, valid for a 100 kHz pixel clock (SCI-SLOW-SPEED)

3.3 HAWAII-2RG Detector characterization using the fast pixel clock

A set of cold dark and flat field exposures was taken with the MATISSE_gen_cal_det_L_FAST OB (21.4.2017 in Nice). The associated MATISSE DRS plug-in *mat_cal_det* was used to calculate the bad pixel map, flat field map and nonlinearity map for the HAWAII-2RG detector at fast speed (2 MHz pixel clock). In addition some characteristic properties were calculated from the plug-in:

- Conversion factor: 2.60 e-/DU
- Readout noise: 53.5 e-
- Bad pixels: 13619 bad pixels of 2048x2048 pixels
- MINDIT: 0.0782393 s for the whole detector
- Full well capacity: 130000 e-
- Nonlinearity compensation: up to 100000 e- possible, max residual 1 %
- Dark current: 0.022 e-/s (data sheet), < 1 e-/s (estimated, includes stray light)
- Stray light: about 3200 s until stray light reaches RON^2
- Masked area: left=80, right=80, bottom=30, top=40

The HAWAII-2RG detector shows 275 compact clusters of at least 3 bad pixels and three loose clusters of bad pixels:

- a large loose cluster at (294,1907), 32 pixel diameter, 244 bad pixels
- a large loose cluster at (327,1092), 26 pixel diameter, 178 bad pixels
- a large loose cluster at (1634,1224), 50 pixels diameter, 155 bad pixels
- 3449 clusters of 2 bad pixels
- 150 clusters of 3 bad pixels
- 76 cluster of 4 bad pixels
- 16 clusters of 5 bad pixels
- 6 clusters of 6 bad pixels
- 8 clusters of 7 bad pixels
- 7 clusters of 8 bad pixels
- 2 clusters of 9 bad pixels
- 2 clusters of 18 bad pixels
- single cluster with 11, 12, 19, 20, 24, 26, 32 and 52 bad pixels

The following image shows the bad pixel map estimated from data taken in Nice, 21. April, 2017.

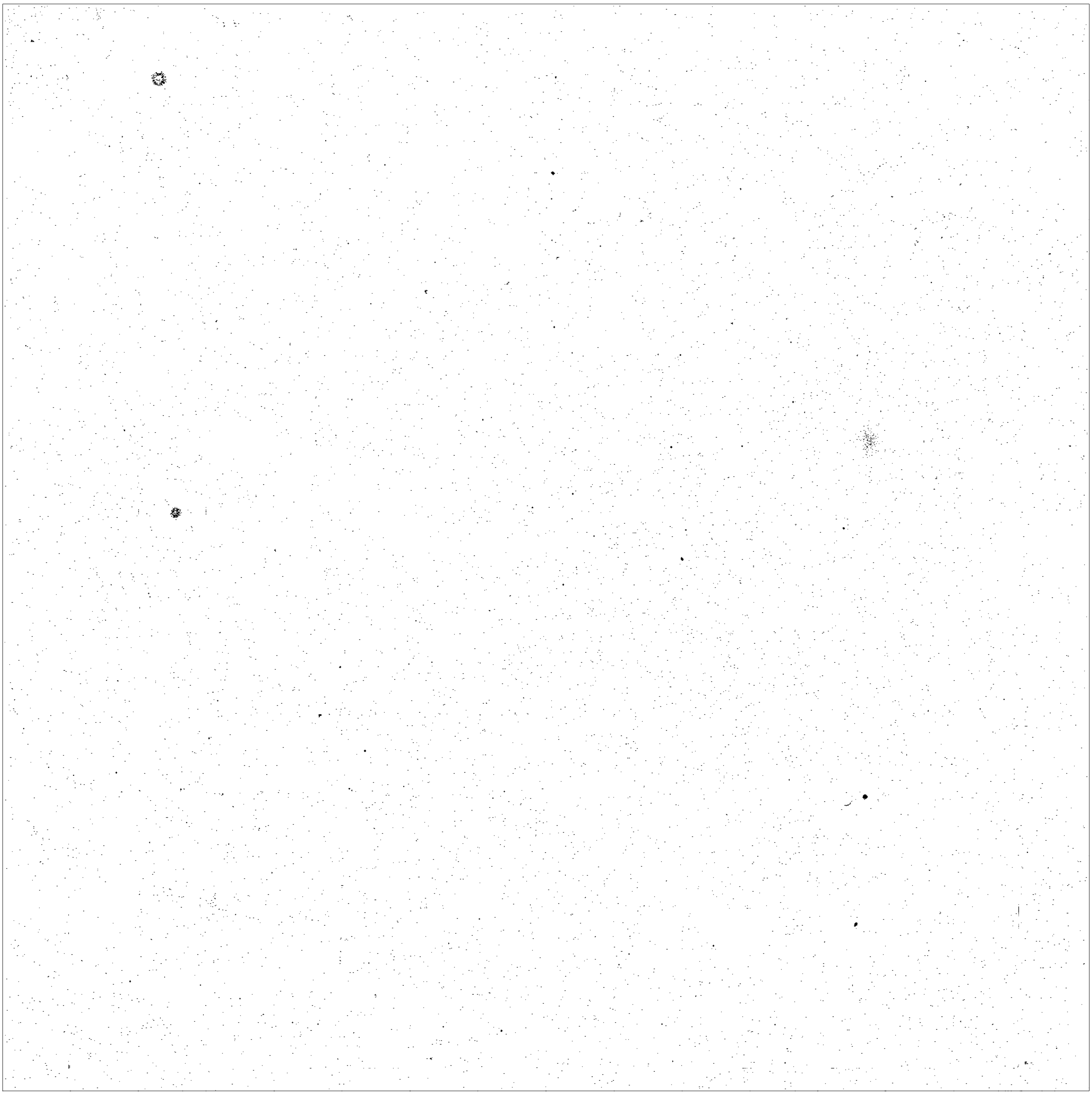

Illustration 2: HAWEAII-2RG bad pixel map, valid for a 2 MHz pixel clock (SCI-FAST-SPEED)

3.4 Aquarius Detector characterization using the low gain mode

- Conversion factor (12.27): 190 e-/DU
- Readout noise: 1800 e-
- Bad pixels: 321 bad pixels of 1024x1024 pixels
- MINDIT: 50 µs, <10 ms for reading the whole detector
- Full well capacity: 9000000 e-
- Nonlinearity compensation: up to 6000000 e- possible, max residual 1 %
- Dark current: 200 e-/s @ 8.5 K (data sheet, no stray light), 13000 e-/s (estimated, includes stray light)
- Masked area: left=32, right=32, bottom=32, top=31

It was not possible to calculate the conversion factor using the plug-in due to the ELFN which influences the measured temporal variance. Instead the conversion factor was calculated from the electronic amplification, electron charge, capacity of a pixel unit cell and ADC characteristics.
The Aquarius detector shows 29 compact clusters of at least 3 bad pixels:

- 19 clusters of 2 bad pixels
- 6 clusters of 3 bad pixels
- 3 clusters of 4 bad pixels
- 2 clusters of 5 bad pixels
- 4 clusters of 6 bad pixels
- 3 clusters of 7 bad pixels
- 2 clusters of 9 bad pixels
- 2 clusters of 12 bad pixels
- 2 clusters of 17 bad pixels
- single cluster with 8, 10, 13, 26 and 36 bad pixels

The following image shows the bad pixel map estimated from data taken in Nice, 15. July, 2016.

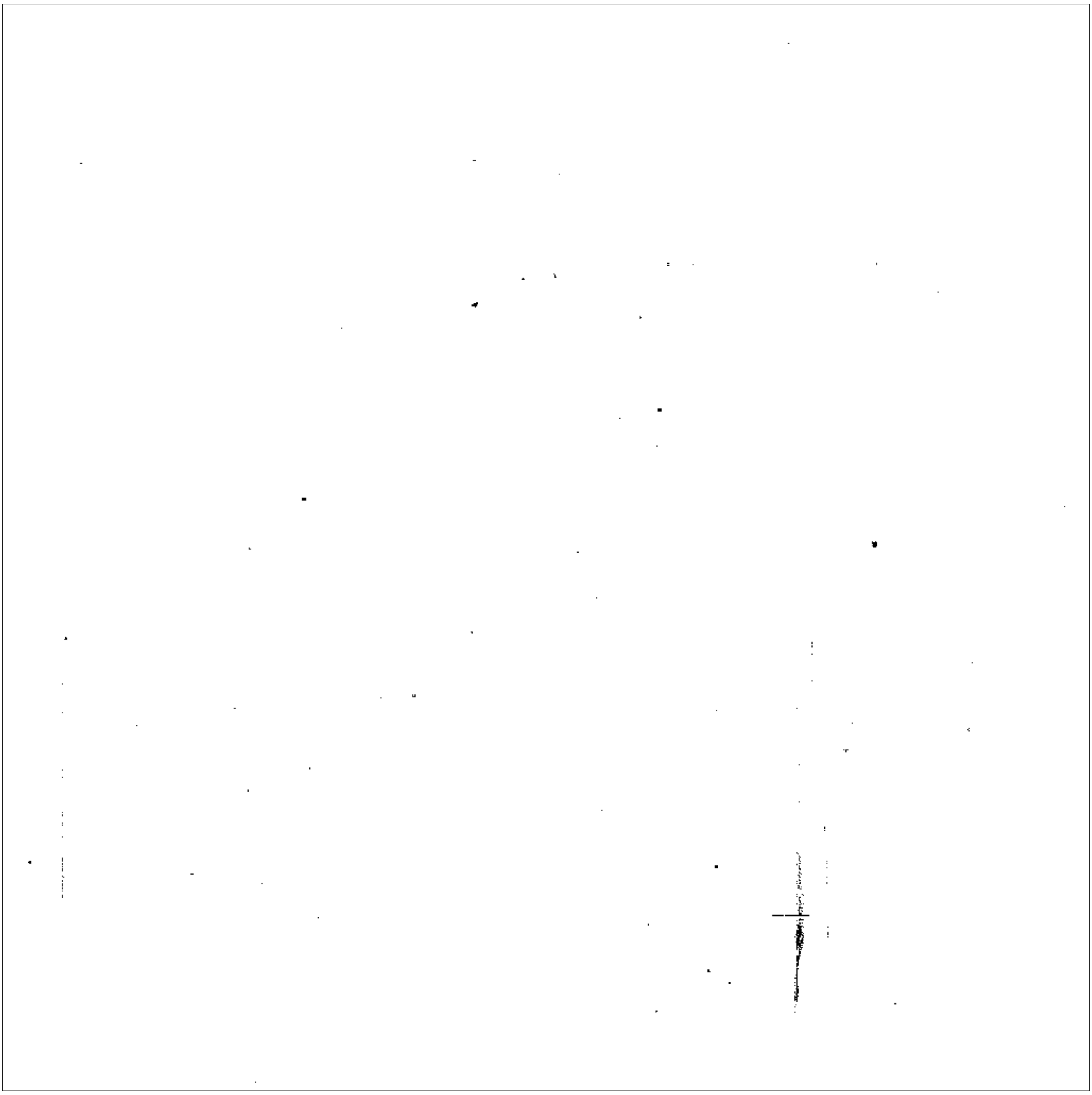

Illustration 3: Aquarius bad pixel map, valid for low gain (SCI-LOW-GAIN)

The vertical stripes with many bad pixels are between the interferometric and photometric channels. Since these pixel are not well illuminated, additional bad pixels are found (false positives).

3.5 Aquarius detector characterization using the high gain mode

- Conversion factor(12.27): 20 e-/DU
- Readout noise: 210 e-
- Bad pixels: 753 bad pixels if 1024x1024 pixels
- MINDIT: 50 µs, <10 ms for reading the whole detector
- Full well capacity: > 960000 e-
- Nonlinearity compensation: up to 960000 e- possible, max residual 1 %
- Dark current: 200 e-/s @ 8.5 K (data sheet, no stray light), 13000 e-/s (estimated, includes stray light)
- Masked area: left=32, right=32, bottom=32, top=31

The conversion factor was calculated using the detector properties directly (same reason as for the low gain mode).
The Aquarius detector shows 67 compact clusters of at least 3 bad pixels:

- 38 clusters of 2 bad pixels
- 24 clusters of 3 bad pixels
- 9 clusters of 4 bad pixels
- 9 clusters of 5 bad pixels
- 3 clusters of 6 bad pixels
- 4 clusters of 7 bad pixels
- 2 clusters of 8 bad pixels
- 2 clusters of 9 bad pixels
- 2 clusters of 13 bad pixels
- 2 clusters of 19 bad pixels
- 2 clusters of 26 bad pixels
- single cluster with 10, 12, 14, 15, 16, 17, 24 and 40 bad pixels

The following image shows the bad pixel map estimated from data taken in Nice, 21. April, 2017.

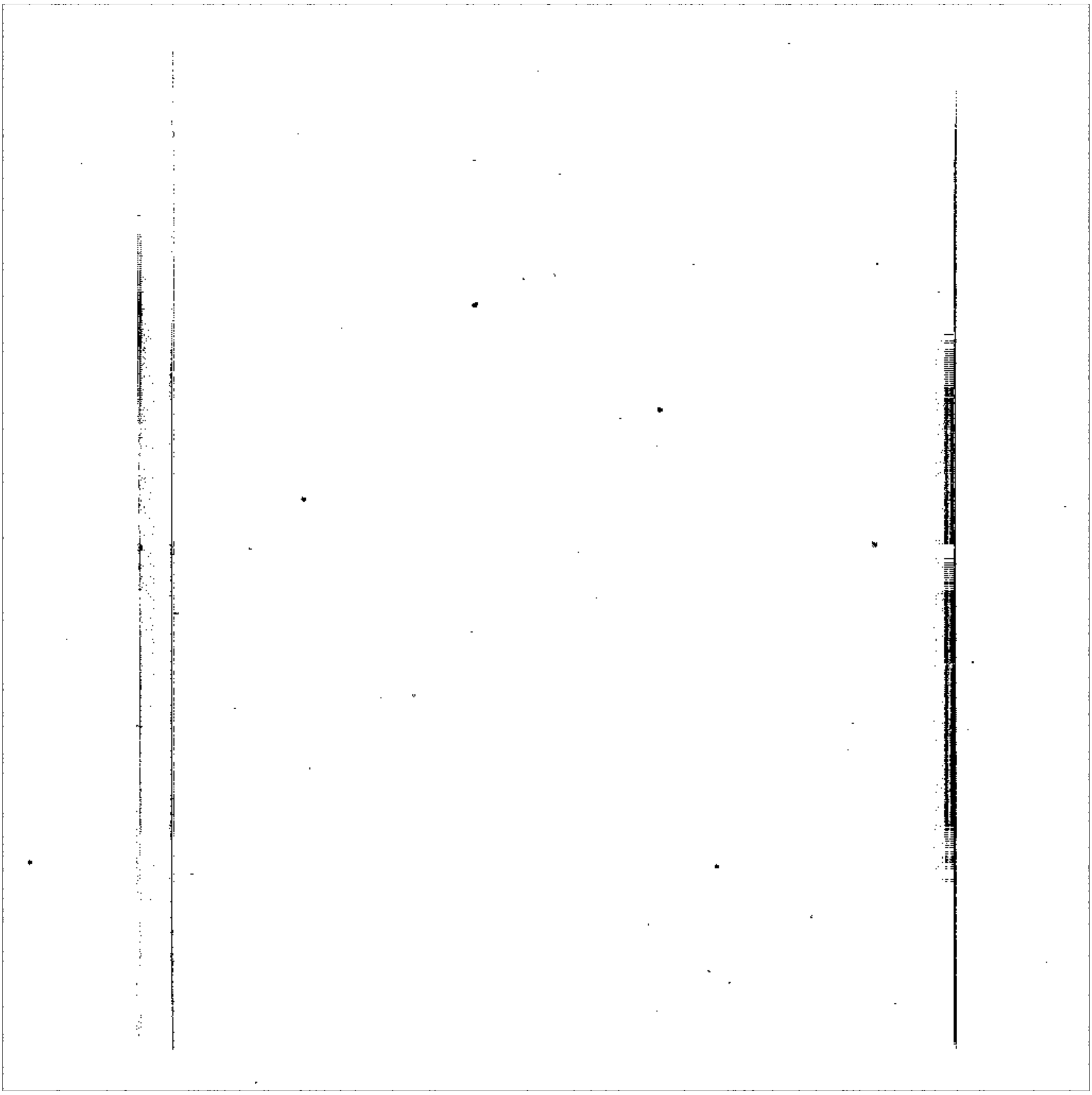

Illustration 4: Aquarius bad pixel map, valid for high gain (SCI-HIGH-GAIN)

The vertical stripes with many bad pixels are between the interferometric and photometric channels. Since these pixel are not well illuminated, additional bad pixels are found (false positives).

3.6 Remanence measurements

Test setup:

- L-Band, HAWAII-2RG:
  - OB: MATISSE_gen_cal_imrem_L_FAST
  - Readout mode: SCI-FAST-SPEED (2 MHz pixel clock)
  - Place and date: Heidelberg, 16. October 2014
  - TDELAY: 0 – 30 ms
  - plug-in: mat_im_rem
- N-Band, Aquarius:
  - OB: MATISSE_gen_cal_imrem_N_HIGH
  - Readout mode: SCI-HIGH-GAIN (high gain)
  - Place and date: Heidelberg, 15. April 2014
  - TDELAY: 0 – 30 ms
  - plug-in: mat_im_rem

The following plots show the calculated values.

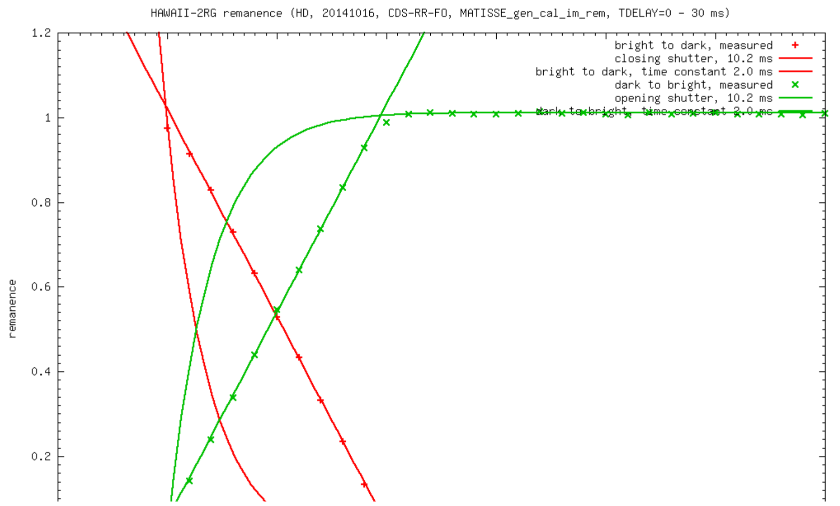

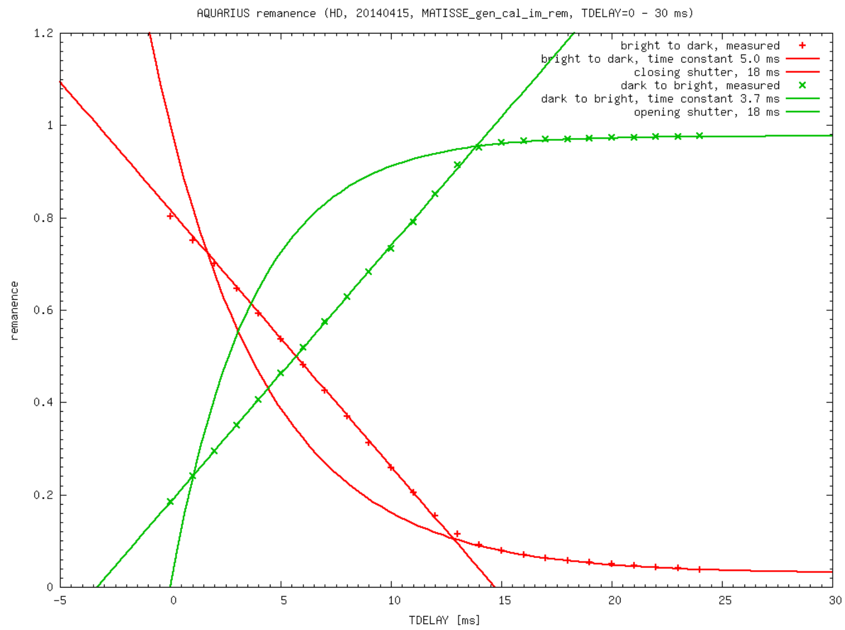

Illustration 6: N-Band, Aquarius, Remanence

Test results:

- HAWAII-2RG, fast shutter open ↔ closed (11.08) 10.2 ms
- Aquarius, fast shutter open ↔ closed (11.08) 18 ms
- HAWAII-2RG, time constant bright ↔ dark (12.24) 2 ms
- Aquarius, time constant bright ↔ dark (12.25) 5 ms

For the HAWAII-2RG detector, a delay between two frames of 8 ms gives a remanence value of 2 %, for the Aquarius detector, a delay between two frames of 20 ms gives a remanence value of 2 %. A special readout timing for the Aquarius (realized as SCI-LOW-GAIN and SCI-HIGH-GAIN readout modes) allows that the time between two exposures is maximized (delay = frame time – read time).
A slightly worse remanence value of 5 % can be achieved by waiting only three time constants. This will result in 6 ms delay for the HAWAII-2RG and 15 ms delay for the Aquarius detector.

3.7 Crosstalk between pixels

The crosstalk between pixels (spatial correlation) is determined by taking a series of flat field frames, calculate the median intensity for each pixel, subtract that from each frame and calculate the autocorrelation using a Fourier method.

Test results:

- HAWAII-2RG, 2 MHz pixel clock spatial=1.3 %, spectral=2.8 %
- HAWAII-2RG, 2 MHz pixel clock spatial=3.4 %, spectral=1.8 %
- Aquarius, high gain mode spatial=8.1 %, spectral=4.8 %
- Aquarius, low gain mode spatial=9.8 %, spectral=6.2 %

In 2015, a test was made until which readout speed the pixel-to-pixel correlation (spatial) for the HAWAII-2RG detector is inside the specification. The result of this test is shown in the following figure:

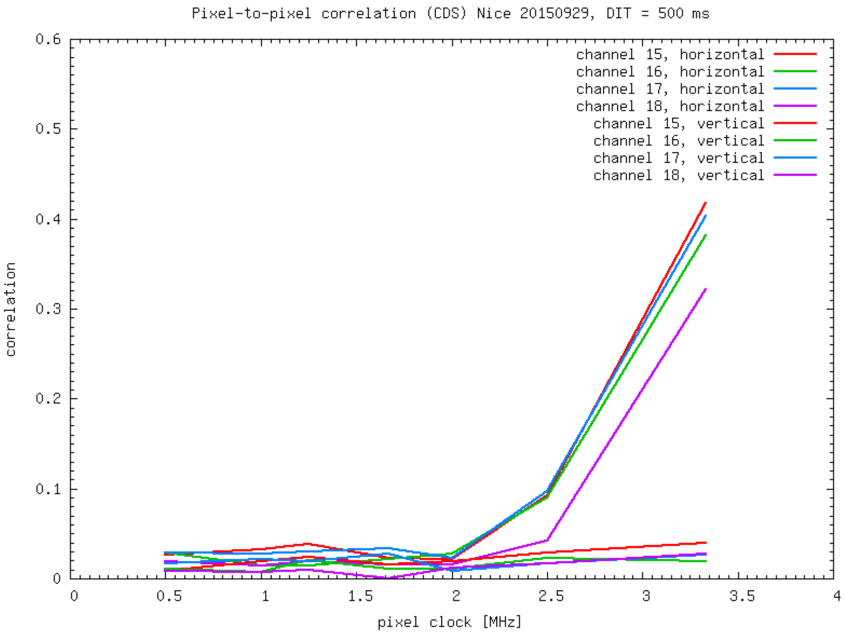

Illustration 7: Spatial correlation for the HAWAII-2RG detector depending on the pixel clock.

The HAWAII-2RG detector can be used up to 2 MHz pixel clock which is the default speed for the SCI-FAST-SPEED readout mode. It is possible to change the pixel clock with the DET.SEQ1.TIMEFAC keyword:

- The TIMEFAC keyword must have a value of 2 or greater!
- The time between two pixels is 0.1 µs * TIMEFAC.
- The default value of 5 gives a pixel clock of 2 MHz.

The Aquarius detector is used with a pixel clock of 2.4 MHz. This will result in pixel crosstalk above specification. It is possible to use a lower pixel clock in order to reach the specification for the horizontal crosstalk:

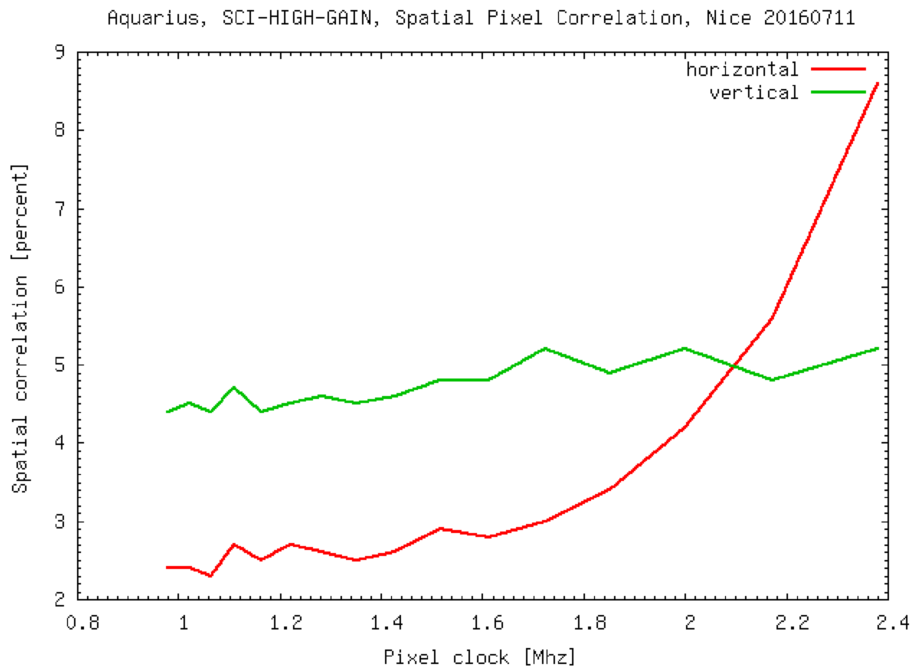

Illustration 8: Aquarius pixel crosstalk, pixel clock dependency

It is possible to change the pixel clock with the DET.SEQ1.TIMEFAC keyword:

- The TIMEFAC must have a value of 8 or greater.
- The time between two pixels is 0.1 us + 0.04 us * TIMEFAC.
- The default value of 8 gives a pixel clock of 2.4 MHz.

A TIMEFAC value of at least 12 (1.7 MHz) will result in a horizontal crosstalk inside specification.

3.8 Temporal stability

The temporal stability describes the variations of the measured signal which are not readout or photon noise. These variations are characterized as Allan Variance or ELFN. The data were taken with the MATISSE_gen_cal_imext_L_FAST and MATISSE_gen_cal_imext_N_HIGH OB.

Test results:

- HAWAII-2RG, 2 MHz pixel clock
  - minimal Allan Variance at 100 seconds (darks)
  - minimal Allan Variance at 75 seconds (flats)
- Aquarius, high gain mode
  - minimal Allan Variance at 110 seconds (darks)
  - minimal Allan Variance at 50 seconds (flats)

3.9 Correlated noise

These noise measurements cover all external interference (noise from other electronic components). It is measured by taking long series of cold dark frames, calculate for each pixel a temporal power spectrum and average them. Peaks in this average power spectrum represent external noise.

Measurements from 15.7.2016 in Nice shows that no correlated noise do exist for the HAWAII-2RG detector at 2 MHz pixel clock. Neither for the fast (horizontal, 2 MHz pixel clock) nor for the slow direction (vertical, about 26 kHz).

Measurements from 28.11.2016 in Nice shows that no correlated noise do exist for the Aquarius detector. Neither for the fast (horizontal, about 2.4 MHz pixel clock) nor for the slow direction (vertical, about 75 kHz).

3.10 Stray light

The HAWAII-2RG shows a stray light intensity below 1 e-/s only if no spectral dispersion is used (INS.DOL = OPEN). If a spectral dispersion is used, the stray light level is even smaller.

The Aquarius detector shows stray light coming from the 36 K warm optics (14.11.2016):

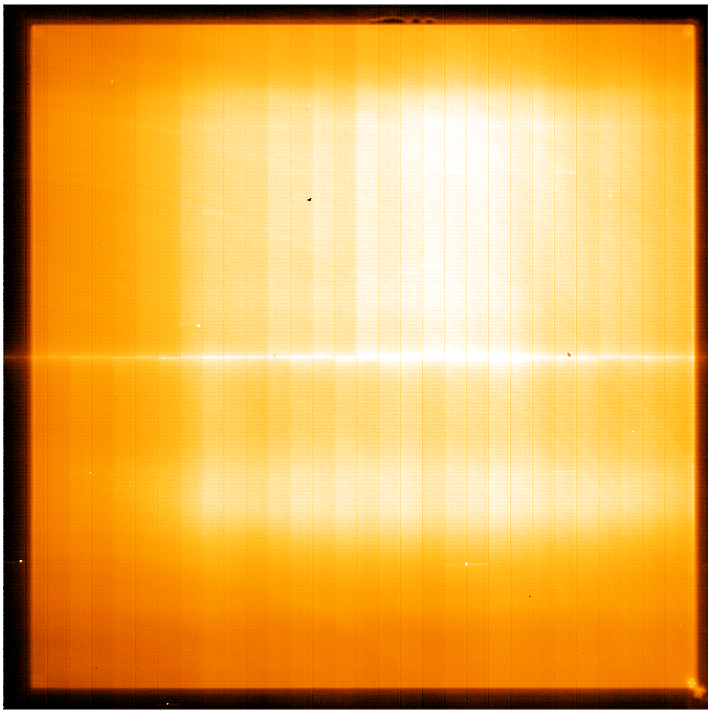

Illustration 9: Aquarius stray light coming from cold optics.

The image is the average of 32 frames with a DIT of 20 s. From such data with different DIT (20 ms, 20 ms, 50 ms, 100 ms, 200 ms, 500 ms, 1 s, 2 s, 5 s, 10 s and 20 s), the following plot can be derived:

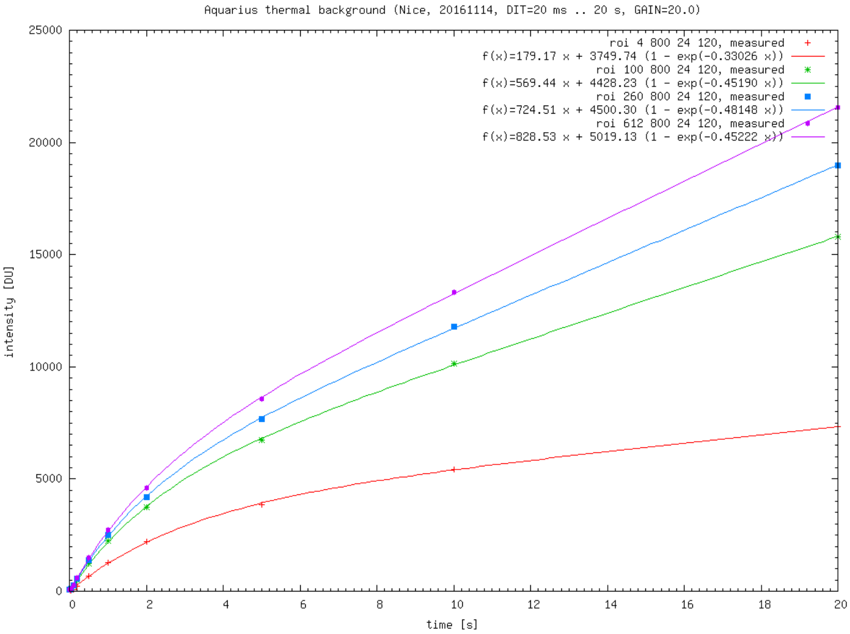

Illustration 10: Aquarius stray light depending from DIT.

This plot shows that with increasing DIT, an offset is introduced into the raw data (red curve) which is compensated for by subtracting the cold darks with the same DIT. If, for example, from the magenta colored curve the red curve is subtracted, this difference gives a stray light estimation for that region (24x120 pixels at (612, 800)). Therefore the stray light for the Aquarius, at this bright part, is about (830 - 180)*20 = 13000 e-/s.

3.11 Nonlinearity

The HAWAII-2RG detector shows an intensity (measured DU) dependent nonlinearity which is determined for each illuminated pixel. The measurements are made with DIT between 100 ms and 30 s for both readout speeds. For each pixel, the individual measurements are fitted with the function

$$I_{cal} = a * I_{raw} + b * e^{(I_{raw} - c) * d}$$

and the coefficients stored in a static nonlinearity map. In addition, the maximum intensity is estimated for which the function represents the measurements with a given accuracy. The next plot shows the nonlinearity function for three pixels. The data samples at about 50000 DU represents the maximum value in the data. This plot shows that the nonlinearity compensation does not include the individual pixel gain. This is covered by the static flatfield map.

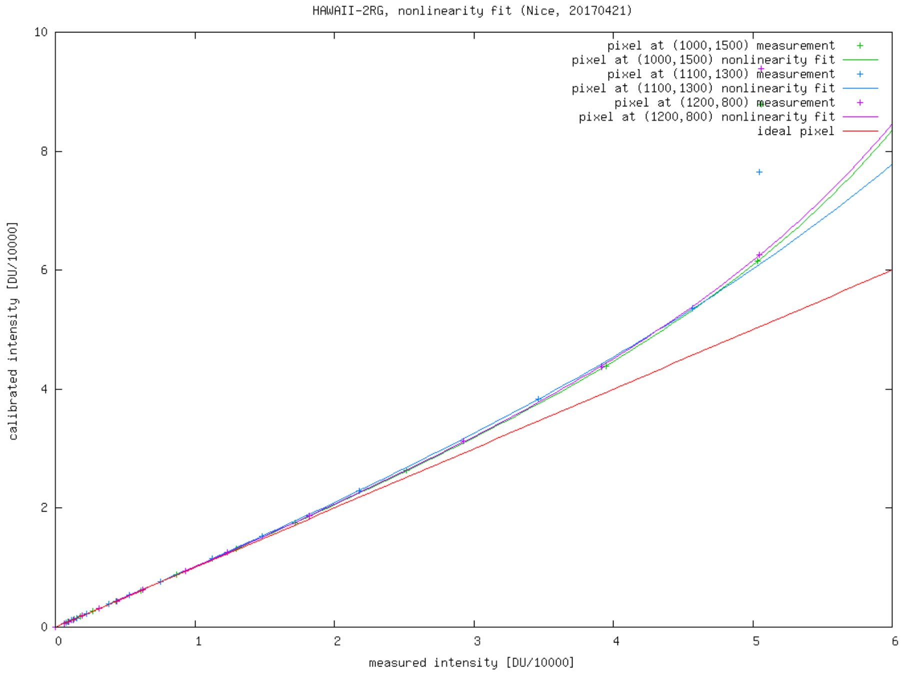

Illustration 11: HAWAII-2RG, nonlinearity fit for three pixels at 2 MHz pixel clock

The Aquarius detector shows a flux (measured DU/s) dependent nonlinearity. This leads to static nonlinearity maps which are valid only for one specific DIT. The following plot shows the mapping from raw to calibrated values for different DIT, this mapping is used for all pixels:

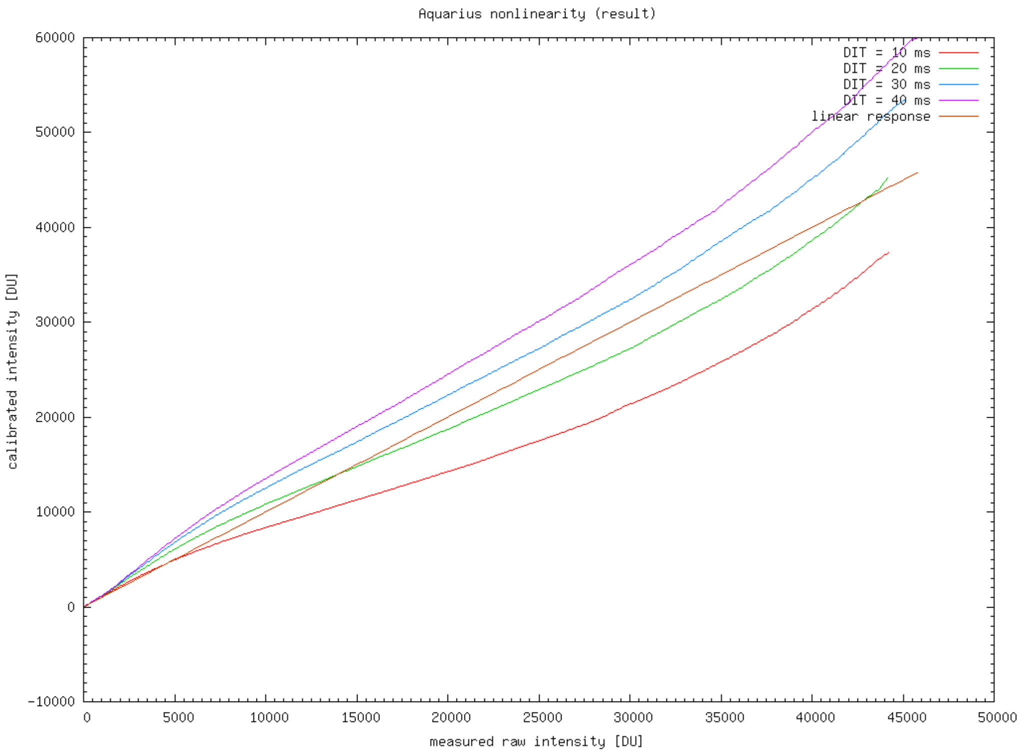

Illustration 12: Aquarius nonlinearity for several DIT

3.12 Detector vibration

In Heidelberg, February 24., 2014, measurements with the Aquarius detector were made in order to estimate the vibration of the detector related to the rest of the instrument. Common mode vibrations cannot be detected by this kind of measurements. An instrument setup was selected which projects small slits on the detector:

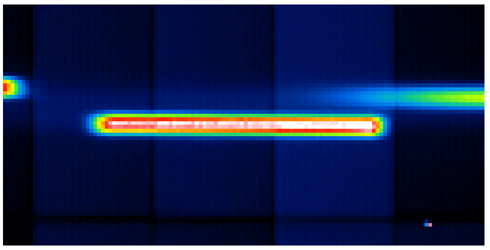

Illustration 13: Aquarius, slit for vibration measurements

On the left side of the slit image, the intensity goes from 0 to about 25000 DU. For each of these pixels, the median intensity and the temporal variance is calculated from a series of 2000 frames. If the image on the detector changes its position caused by vibrations, the calculated variance for each of the pixel will be higher than expected. On the left side of the slit, pixels show the following intensities and variances:

x position	intensity [DU]	variance [DU^2]	photon noise [DU^2]
180 - 189	0	0	0
190	-37	5	-2
191	290	13	14
192	542	46	27
193	1598	188	80
194	3467	620	173
195	6636	1334	332
196	10749	2612	537
197	15509	4792	775
198	19620	5143	981
199	22847	7592	1142
200	24575	5726	1229
201	25362	5464	1268
202 - 211	24823	6910	1241

Table 2: Aquarius vibration measurements at left edge of slit image

Near the center of the edge, a pixel shows an intensity of 15500 DU (marked with blue), the observed variance is 4800 DU^2. From the measured intensity and a conversion factor of 20 e-/DU, the expected variance is 775 DU^2.

Two sources for an additional variance do exist:

1. The variance will be higher than the photon noise due to ELFN.
2. The variance will be higher than the photon noise, if the image on the detector changes its position due to vibrations.

It is not possible to distinguish between these two effects using the instrument setup.

Upper limits for the vibrations can be estimated under the assumption that a sinusoidal vibration is assumed and the effects of such a vibration for different frequencies and peak-to-valley values is compared with the measured variance:

Frequency [Hz]	Jitter, peak-to-valley [µm]					
	0.5	1.0	1.3	1.5	1.7	2.0
1	1388.3	3291.4	5033.4	6446.5	8068.8	108708
2	1375.7	3240.5	4956.4	6352.3	7949.1	10705.2
5	1382.4	3257.3	4995.1	6400.0	8002.1	10784.8
10	1376.6	3246.1	4970.7	6366.9	7972.2	10746.9
20	1368.3	3215.0	4910.5	6286.8	7864.8	10593.5
50	1303.1	2947.0	4482.0	5705.5	7129.8	9566.1
100	1116.6	2210.4	3224.5	4040.2	4982.1	6587.8

Table 3: Aquarius detector vibration limits (valid for a pixel intensity of 15000 DU)

This table shows that for frequencies below 100 Hz (the detection limit for the measurements), the jitter must be smaller than 1.7 µm. Larger (sinusoidal) vibrations would lead to variances higher than measured. Due to the unknown ELFN component, the realistic vibration limit is even lower than 1.7 µm.
The following plot shows the temporal power spectrum at the lower side of the slit (10 pixels with an average intensity of about 10000 DU) and the right side of the slit (3 pixels with an average intensity of about 10000 DU).

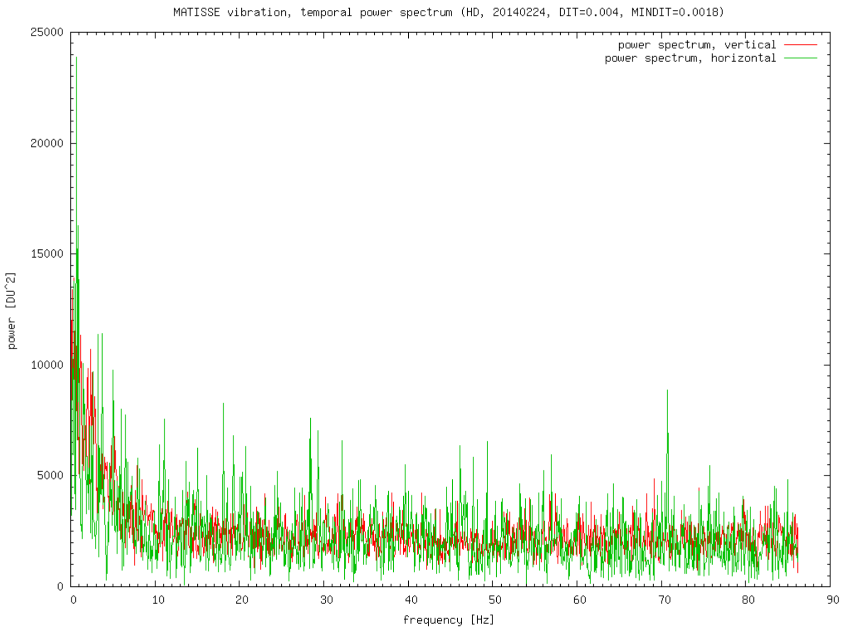

Illustration 14: Aquarius, vibration measurements via temporal power spectra

If the image position in the detector would change due to vibration, the pixels on the outer side of the slit would not only show a higher variance, but also a power spectrum showing peaks at some frequencies. A total erratic change of the image position is very unlikely.

Both power spectra do not show any obvious peaks but a higher than expected white noise plateau. The cause of this is the excess noise of the Aquarius detector which has a low frequency component (ELFN) and a white noise component. The white noise in the power spectrum is at about 2600 DU^2. This number is equal with the variance measurements for a pixel at about 10000 DU (marked with green). Therefore no image position changes due to vibration can be detected.

APPENDIX: Abbreviations and Acronyms

This document employs several abbreviations and acronyms to refer concisely to an item, after it has been introduced. The following list is aimed to recall the extended meaning of each short expression:

AD	Applicable Document
AMO	Analysis Modules
ARC	Artificial Sources
BCD	Beam Commutating Device
CAU	Control and Alignment Unit
COB	Cold Optics Bench
COL	Collimating optics
CPL	Co-Phasing Unit – L band
CPN	Co-Phasing Unit – L band
CUL	Co-alignment Unit – L band
CUN	Co-alignment Unit – N band
DCS	Detector Control System
DET	DETector
DIT	Detector Integration Time
DRS	Data Reduction System
DU	Digital Unit
ELFN	Excess Low Frequency Noise
IRS	Infrared Source
MAIT	Manufacturing Alignment Integration and Tests
MAS	Mask
MATISSE	Multi-AperTure mid-Infrared SpectroScopic Experiment
MRI	Mirror Input
MRO	Mirror Output
MRR	MATISSE Readiness Review
OB	Observing Block
OCA	Observatoire de la Côte d'Azur
OML	OPD modulator – L band
OMN	OPD modulator – N band
OPD	Optical Path Difference
OPL	Optical Path Length
PAE	Preliminary Acceptance Europe
PAO	Photometry Anamorphic Optics
PMR	Primary Mirror
PSF	Point Spread Function
PUC	Pupil Creator
PV	Peak To Valley
QE	Quantum Efficiency
RD	Reference Document
RMS	Root Mean Square
RON	Read Out Noise
SMR	Secondary mirror
SOA	Source Analysis
SOS	Source Selector
SR	Strehl Ratio
TBC	To Be Clarified
VAS	Visible Alignment Source
VLT	Very Large Telescope
WFA	Wavefront Analyzer
WFE	Wavefront Error
WOP	Warm Optics

End of document